



**HAL**  
open science

## Laser ablation of Ga-Sb-Te thin films monitored with quadrupole ion trap time-of-flight mass spectrometry

Govinda Mandal, Magdalena Gorylova, Virginie Nazabal, Petr Nemeč, Josef Havel

► **To cite this version:**

Govinda Mandal, Magdalena Gorylova, Virginie Nazabal, Petr Nemeč, Josef Havel. Laser ablation of Ga-Sb-Te thin films monitored with quadrupole ion trap time-of-flight mass spectrometry. *Journal of the American Ceramic Society*, 2021, 104 (12), pp.6643-6652. 10.1111/jace.18021 . hal-03331051

**HAL Id: hal-03331051**

**<https://hal.science/hal-03331051>**

Submitted on 8 Sep 2021

**HAL** is a multi-disciplinary open access archive for the deposit and dissemination of scientific research documents, whether they are published or not. The documents may come from teaching and research institutions in France or abroad, or from public or private research centers.

L'archive ouverte pluridisciplinaire **HAL**, est destinée au dépôt et à la diffusion de documents scientifiques de niveau recherche, publiés ou non, émanant des établissements d'enseignement et de recherche français ou étrangers, des laboratoires publics ou privés.

DR PETR NEMEC (Orcid ID : 0000-0003-2426-3078)

PROFESSOR JOSEF HAVEL (Orcid ID : 0000-0002-6675-5671)

Article type : Research Article

## **Laser ablation of Ga-Sb-Te thin films monitored with quadrupole ion trap time-of-flight mass spectrometry**

**Govinda Mandal<sup>1</sup>, Magdaléna Gorylová<sup>3</sup>, Virginie Nazabal<sup>2,3</sup>, Petr Němec<sup>3</sup>, Josef Havel<sup>1\*</sup>**

<sup>1</sup>Department of Chemistry, Faculty of Science, Masaryk University, C14/326-Kamenice 753/5, 625 00 Brno, Czech Republic

<sup>2</sup>Univ Rennes, CNRS, ISCR UMR6226, ScanMAT UMS 2001, F-35000 Rennes, France

<sup>3</sup>Department of Graphic Arts and Photophysics, Faculty of Chemical Technology, University of Pardubice, Studentská 573, 53210 Pardubice, Czech Republic

### **Abstract**

Laser ablation of Ga-Sb-Te chalcogenide thin films prepared by radio-frequency magnetron co-sputtering was monitored with quadrupole ion trap time of flight mass spectrometry (QIT TOF MS). The mass spectra of eleven thin films of various composition (Ga: 0-53.1, Sb: 0-52.0, and Te: 0-100.0 at. %) were recorded. Several series of unary ( $\text{Ga}_x$ ,  $\text{Sb}_y$ , and  $\text{Te}_z$ ) binary ( $\text{Ga}_x\text{Sb}_y$ ,  $\text{Ga}_x\text{Te}_z$ , and  $\text{Sb}_y\text{Te}_z$ ), and ternary  $\text{Ga}_x\text{Sb}_y\text{Te}_z$  clusters were identified in both positive and negative ion modes. Stoichiometry of observed clusters was determined. Up to 18 binary clusters (positively and negatively charged) were detected for thin film with low Sb content of 6.5 at. %. The highest number (4) of ternary clusters was observed for thin film with high Te content of 66.7

This article has been accepted for publication and undergone full peer review but has not been through the copyediting, typesetting, pagination and proofreading process, which may lead to differences between this version and the [Version of Record](#). Please cite this article as [doi: 10.1111/JACE.18021](https://doi.org/10.1111/JACE.18021)

at. %. The number of generated clusters and their peaks intensity varied according to the chemical composition of thin films. Altogether, 41 clusters were detected. The laser ablation monitoring shows laser-induced fragmentation of thin film structure. The relation of clusters stoichiometries to the chemical composition of thin films is discussed. The fragmentation can be diminished by covering a surface of thin films with paraffin's, glycerol, or trehalose sugar thin layers. The stoichiometry of generated clusters shows partially structural characterization of thin films.

#### **KEYWORDS**

Ga-Sb-Te, thin films, clusters, laser ablation, amorphous chalcogenides, quadrupole ion trap time-of-flight mass spectrometry, diminishing clusters fragmentation

*\*Correspondence to:* Josef Havel; e-mail: [havel@chemi.muni.cz](mailto:havel@chemi.muni.cz)

## 1 | INTRODUCTION

During the last decades, Ge-Sb-Te thin films have attracted attention due to their ability to transition quickly and reversibly between their amorphous and crystalline phases. Hence, they have wide applications in phase change memories,<sup>1-4</sup> thermal energy storage,<sup>5</sup> photonics,<sup>6</sup> holography,<sup>7</sup> and so forth.

To improve the properties of Ge-Sb-Te phase change materials, their chemical composition can be altered using two approaches. First, the composition is modified. For example, Ge-Sb-Te compounds, along with the pseudo-binary GeTe-Sb<sub>2</sub>Te<sub>3</sub> tie line, which includes Ge<sub>1</sub>Sb<sub>2</sub>Te<sub>4</sub> and Ge<sub>8</sub>Sb<sub>2</sub>Te<sub>11</sub>, were investigated apart from the prototypical Ge<sub>2</sub>Sb<sub>2</sub>Te<sub>5</sub> composition.<sup>8,9</sup> In the other approach, they are doped or alloyed with other elements. For example, the Ge and Te in Ge<sub>8</sub>Sb<sub>2</sub>Te<sub>11</sub> material were partially replaced by Sn and Se, respectively. Such prepared thin films demonstrate high electrical and reflectivity contrasts between their crystalline and amorphous phases.<sup>10</sup>

Apart from the Ge-Sb-Te system, the Ga-Sb-Te system has been studied bearing in mind applications in the field of phase change memories<sup>11-16</sup> or infrared thermal detectors.<sup>17</sup> Kao et al.<sup>11</sup> fabricated thin films composed of active Ga<sub>2</sub>Sb<sub>5</sub>Te<sub>3</sub> material using radio-frequency (RF) magnetron sputtering technique and suggested that the prepared thin films demonstrated the ability to make three-level resistance changes in a single memory unit to facilitate a higher memory capacity. Furthermore, the other authors have used the magnetron co-sputtering technique with GaSb and Sb<sub>8</sub>Te<sub>2</sub>,<sup>12</sup> GaSb, Sb, and Te,<sup>13</sup> and GaSb and Sb<sub>2</sub>Te<sub>3</sub><sup>14</sup> targets for the fabrication of thin films and reported that such thin films present high crystallization speeds, high electrical contrasts between crystalline and amorphous phases and usually exhibit promising characteristics for novel phase change memories. Lee et al. showed that among the various composition of films studied in their work,<sup>18</sup> the Ga<sub>6.3</sub>Sb<sub>68.0</sub>Te<sub>25.7</sub> film has the shortest crystallization time and it has been suggested for application as phase change optical-recording media.<sup>18</sup> Recently, Bouška et al.<sup>16</sup> fabricated Ga-Sb-Te thin films using RF magnetron co-sputtering with GaTe and Sb<sub>2</sub>Te<sub>3</sub> targets pointing out large values of optical contrast in fabricated layers, which might be in some cases even higher than those of the Ge-Sb-Te system. It is worth noting that apart from RF magnetron (co)-sputtering, chalcogenide thin films can be generally fabricated by a variety of deposition methods, such as pulsed laser deposition,<sup>19</sup> chemical bath deposition,<sup>20</sup> thermal evaporation,<sup>21</sup> etc.

After laser-induced crystallization, the phase change optical disks exploiting Ga-Sb-Te media with composition located along the  $\text{Sb}_7\text{Te}_3$ -GaSb and  $\text{Sb}_2\text{Te}_3$ -GaSb pseudo-binary tie lines have a single hexagonal phase. The values of lattice parameters of this phase are responsible for the writability and erasability capacities of optical disks.<sup>22</sup> Furthermore, amorphous  $\text{Ga}_4\text{Sb}_6\text{Te}_3$  phase change alloy has been investigated using first-principles molecular dynamics simulations within the density functional theory framework to elucidate its structure. The most abundant bonds, such as Ga-Sb and Ga-Te, are observed, while only a few Sb-Te bonds contribute to the alloy network. There are two different structural configurations, namely, a tetrahedral-like geometry formed by Ga and four-coordinated Sb atoms, and a pyramidal geometry formed by three-coordinated Sb atoms, in the  $\text{Ga}_4\text{Sb}_6\text{Te}_3$  phase change alloy.<sup>23</sup>

Previous studies have shown that laser ablation time-of-flight mass spectrometry is a suitable technique for the generation and characterization of clusters formed from chalcogenide glasses or their thin films during interaction with laser pulses, which are present in plasma plume.<sup>24–26</sup> Houška et al.<sup>27</sup> investigated  $\text{Ge}_2\text{Sb}_2\text{Te}_5$  thin film and  $\text{Sb}_2\text{Te}_3$  bulk material using mass spectrometry and identified  $\text{SbTe}_2$ ,  $\text{Sb}_2\text{Te}$ , and  $\text{Sb}_3\text{Te}$  clusters for thin film and  $\text{TeSb}$ ,  $\text{TeSb}_2$ , and  $\text{TeSb}_3$  clusters for bulk material. Mawale et al.<sup>25</sup> studied Ga-Sb-Se thin film and reported various  $\text{Ga}_x\text{Se}_z$ ,  $\text{Sb}_y\text{Se}_z$ , and  $\text{Ga}_x\text{Sb}_y\text{Se}_z$  clusters. Interestingly, no  $\text{Ga}_x\text{Sb}_y$  clusters were detected in this work. However, the Ga-Sb-Te ternary system has not been studied via mass spectrometry as yet.

Matrix free laser desorption ionization or laser ablation (LA) mass spectrometry may generally suffer from the fact that the original structure of glass or inorganic polymer is often substantially fragmented, and the clusters formed can undergo further fragmentation in plasma plume. We have found recently that this undesirable effect can be strongly minimized or eliminated using some inert materials or energy absorbers as a matrix. For example, when a diluted solution of paraffin in xylene was applied on the surface of thin films and dried, higher intensity of mass spectra or clusters of higher mass were observed.<sup>25,28,29</sup> Increased intensities of mass spectra and some new bismuth selenide clusters ( $\text{BiSe}^-$ ,  $\text{BiSe}_2^-$ ,  $\text{BiSe}_3^-$ ,  $\text{BiSe}_4^-$ ,  $\text{Bi}_2\text{Se}_2^-$ ,  $\text{Bi}_2\text{Se}_3^-$ , and  $\text{Bi}_2\text{Se}_4^-$ ) were observed from bismuth selenide thin film coated with paraffin's.<sup>28</sup> Similarly, trehalose sugar has also been reported as a fragmentation diminishing agent.<sup>30</sup> Based on above-described facts we will also examine the effect of these materials or some other energy absorbers for the suppression of fragmentation.

Based on the information summarized above, we have studied in this work the stoichiometries of the  $\text{Ga}_x\text{Sb}_y\text{Te}_z$  clusters generated from the Ga-Sb-Te thin films of different chemical

composition and discussed the relationship between the observed clusters stoichiometries and their parent thin film composition.

## **2 | EXPERIMENTAL PROCEDURE**

### **2.1 | Chemicals**

Polycrystalline GaSb (99.999 %), GaTe (99.999 %), and Te (99.99 %) sputtering targets (2'' diameter, 1/8'' thick) were purchased from ALB Materials, Inc. (Henderson, NV, USA). Single crystalline silicon wafer <100> substrates for thin film deposition were purchased from ON Semiconductors (Czech Republic). Water was double distilled using a quartz apparatus from Heraeus Quarzschmelze (Hanau, Germany). Acetonitrile, acetone, methanol, and trehalose sugar were purchased from Sigma-Aldrich (Steinheim, Germany). Parafilm was obtained from Pechiney Plastic Packaging Inc. (Chicago, USA). Xylene and glycerol were purchased from Lach-Ner (Neratovice, Czech Republic). Red phosphorus was obtained from Riedel de Haën (Hannover, Germany). Micro-90 cleaning agent was purchased from Kratos (Manchester, UK).

### **2.2 | Preparation of thin films**

The RF magnetron co-sputtering of Ga–Sb–Te thin films was performed at room temperature using the MPE600 multi-chamber deposition system (Plassys-Bestek). The experimental conditions of the deposition process are described elsewhere.<sup>31</sup> The chemical composition of the thin films was tailored by varying the RF power (0-35, 0-23, and 0-15 W for the GaSb, GaTe, and Te cathodes, respectively).

### **2.3 | Sample preparation for mass spectrometry**

The thin films were fixed on the target plates, i.e., small pieces of adhesive tape were used to affix the edges of the Si substrates with Ga-Sb-Te films. Afterward, the target with the samples loaded was introduced into the mass spectrometer, where the mass spectra were recorded when the vacuum level was below  $4 \times 10^{-5}$  Pa. Eventually, before loading the samples to the mass spectrometer, the surface of thin films was covered with 0.5  $\mu$ L solutions of some energy absorber materials like glycerol, paraffin's [1 cm<sup>2</sup> parafilm (13 mg) dissolved in 1 mL of xylene], or trehalose sugar saturated solution in acetonitrile. After drying the solutions on the surface of the thin films, the mass spectra were recorded as above.

### **2.4 | Mass spectrometry**

Mass spectra were measured using AXIMA Resonance mass spectrometer (nitrogen pulsed laser emitting at 337 nm) from Kratos Analytical Ltd. (Manchester, UK). The laser energy used ranged from 0 to 180 a.u. (arbitrary units). The repetition mode of experiments was performed at a frequency of 5 Hz and a pulse time width of 3 nanoseconds. The irradiated spot size was about 150  $\mu\text{m}$  in diameter and the maximum laser power was 6 mW (180 a.u.). The resulting laser energy fluence was  $\sim 1 \text{ J}\cdot\text{cm}^{-2}$ . Mass spectra were acquired using at least 2000 laser shots in both reflectron positive and negative ion modes.

### **2.5 | Scanning electron microscopy with energy dispersive X-ray spectroscopy and X-ray diffraction**

A scanning electron microscope (SEM, JEOL JSM 6400) was employed for the study of surface morphology and an energy dispersive X-ray analyzer (EDS) was used to determine the chemical composition of the fabricated thin films. The EDS measurements were done at 3 spots per sample and averaged. The uncertainty of EDS for the studied films was  $\pm 1$  at. %. The X-ray diffraction (XRD) technique (Rigaku MiniFlex 600, Japan) was used to determine the structures of the deposited thin films via  $\text{CuK}\alpha$  radiation. With respect to the incidence beam ( $6^\circ$  below the horizontal direction), the sample was rotated by  $\theta$  and the detector by  $2\theta$ . The diffraction angles were measured at room temperature from  $5$  to  $90^\circ$  ( $2\theta$ ) in  $0.02^\circ$  steps.

### **2.6 | Software and computation**

Theoretical isotopic patterns were calculated using the Launchpad software (Kompact, version 2.3.4, 2003) from Kratos Analytical Ltd. (Manchester, UK). A molecular weight calculator program (version 6.5, 2014) from Pacific Northwest National Laboratory (Richland, WA, USA) was used to estimate the stoichiometries of the clusters.

## **3 | RESULTS**

The review and approach applied to manufacture and characterize Ga-Sb-Te thin films are given in the scheme below:

Fabrication of thin films via RF magnetron co-sputtering using GaSb, GaTe, and Te targets



Characterization of thin films (SEM, EDS, XRD, and Mass spectrometry reflectron positive and negative ion modes)



Mass spectra analysis (clusters stoichiometry determination)

### Scheme of thin films characterization

The chemical composition of the fabricated thin films **A-K** determined via EDS is visualized in the ternary phase diagram (Figure 1) and summarized in Table 1. The co-sputtered films covered a broad range of chemical composition: 0-53.1 at. % of Ga, 0-52.0 at. % of Sb, and 0-100.0 at. % of Te (Table 1). The surfaces of the Ga-Sb-Te thin films were characterized via SEM concluding that their surface morphology is of good quality. The thickness of thin films was in the range of ~140-180 nm ( $\pm 2$  nm). The XRD patterns revealed that all the fabricated thin films, excluding tellurium layer, are amorphous in nature.

The mass spectra were recorded via LA for the obtained Ga-Sb-Te thin films of various composition in both positive and negative ion modes. Most of the  $\text{Ga}_x\text{Sb}_y$ ,  $\text{Ga}_x\text{Te}_z$ ,  $\text{Sb}_y\text{Te}_z$ , and  $\text{Ga}_x\text{Sb}_y\text{Te}_z$  clusters were detected in the positive or negative ion modes in the 100-1000  $m/z$  range. The mass spectra recorded in the negative ion mode were more intense and had a slightly higher number of clusters than those recorded in the positive mode. Therefore, most of the results presented here are for the negative ion mode.

The effect of the laser energy in generating  $\text{Ga}_x\text{Sb}_y\text{Te}_z$  clusters from the thin films **A-K** in both positive and negative ion modes was examined. For the positive ion mode, the “optimal” mass spectra with sufficient mass resolutions and the highest numbers of clusters were recorded for a laser energy range of 150-170 a.u. Similarly, in the negative ion mode, a 140-160 a.u. laser energy range was found to be optimal for recording well-resolved mass spectra with the highest numbers of clusters. For example, the effect of the laser energy is shown in Figure 2 for a mass range of 100-400  $m/z$ . It was demonstrated that the intensity of the mass spectra increased up until a laser energy of 160 a.u. Subsequently, the intensity of mass spectra decreased with further increases in laser energy from 160 to 170 a.u., indicating that the clusters decomposed at high laser energy levels.

#### 3.1 | Mass spectra of Ga-Sb-Te thin films measured in positive ion mode

Several series of clusters were observed from thin films **B-K** with Te content of 11.5-100 at. % in positive ion mode. These series of clusters were  $\text{Ga}_x\text{Sb}^+$  ( $x = 1, 2$ ),  $\text{GaSb}_8^+$ ,  $\text{GaTe}_z^+$  ( $z = 1-3$ ),  $\text{Ga}_2\text{Te}_z^+$  ( $z = 1, 2$ ),  $\text{Ga}_3\text{Te}_z^+$  ( $z = 1, 2$ ),  $\text{Sb}_y\text{Te}^+$  ( $y = 1-3$ ),  $\text{SbTe}_2^+$ ,  $\text{GaSbTe}_z^+$  ( $z = 1, 2$ ), and  $\text{GaSb}_2\text{Te}_z^+$  ( $z = 1, 2$ ). As thin film '**K**' contained 100 % Te, only one series of  $\text{Te}_z^+$  ( $z = 1-5$ ) clusters was detected. In addition, some other unary  $\text{Ga}_2^+$  and  $\text{Sb}_y^+$  ( $y = 1, 3, 4, 9$ ) clusters were observed.

The highest number (15 clusters) of binary and ternary clusters was detected for thin film '**J**,' with the highest content of Te (66.7 at. %), while only one binary  $\text{SbTe}^+$  cluster was noted for thin film '**G**,' with the lowest concentration of Te (12.4 at. %). It is also worth to note that no unary and binary clusters were detected for thin film '**A**,' which contained almost equal content of Ga (48.0 at. %) and Sb (52.0 at. %). The  $\text{GaSb}^+$  cluster with the lowest  $m/z$  value was identified for thin film '**B**,' which has the lowest Te content (11.5 at. %). Similarly, the  $\text{GaTe}^+$  and  $\text{SbTe}^+$  clusters have the lowest masses for '**E**,' '**F**,' and '**J**,' thin films which show Te content  $\geq 41.6$  at. %, and the '**C**,' '**D**,' '**H**,' and '**I**' thin films which have Sb content  $\geq 19.6$  at. %, respectively. Meanwhile, the  $\text{Sb}_3\text{Te}^+$  and  $\text{GaTe}_3^+$  clusters with the highest masses were detected for '**B**,' '**C**,' '**E**,' and '**H-J**' thin films (with concentration of Te  $\geq 11.5$  at. %) and '**F**,' which has no Sb content, respectively. The  $\text{GaSb}_8^+$  cluster shows the highest mass generated from thin film '**D**,' which has the lowest Sb content (19.6 at. %). The peaks intensities of the clusters with the lowest masses observed for most of the thin films ('**B**,' '**E**,' '**F**,' '**H**,' and '**J**,' which have the highest content of Te at 11.5-66.7 at. %) were lower than those of the clusters with the highest masses.

### 3.2 | Mass spectra of Ga-Sb-Te thin films measured in negative ion mode

Various series of clusters were recorded from thin films **A-K**, i.e., having Te content in the range 0-100 at. %. For example, a comparison of the mass spectra generated via LA for the thin films in the range  $m/z$  100-400 is shown in Figure 3. Mass spectra recorded for the thin films were more intense for a higher number of clusters in the negative ion mode than in the positive one. A comparison of the mass spectra intensities recorded via LA for thin film '**E**' in both the positive and negative ion modes is shown in Figure 4. Several series of clusters, namely,  $\text{GaSb}_2^-$ ,  $\text{GaSb}_8^-$ ,  $\text{Ga}_2\text{Sb}_{15}^-$ ,  $\text{Ga}_3\text{Sb}_{14}^-$ ,  $\text{Ga}_4\text{Sb}_{13}^-$ ,  $\text{Ga}_6\text{Sb}_5^-$ ,  $\text{Ga}_7\text{Sb}_4^-$ ,  $\text{GaTe}_z^-$  ( $z = 1-4$ ),  $\text{Ga}_2\text{Te}_z^-$  ( $z = 1, 2$ ),  $\text{SbTe}_z^-$  ( $z = 1-3$ ),  $\text{Sb}_2\text{Te}_z^-$  ( $z = 1, 2$ ),  $\text{GaSbTe}_z^-$  ( $z = 2, 3$ ), and  $\text{Ga}_2\text{SbTe}_2^-$  were generated from the thin films. Likewise, unary  $\text{Ga}_x^-$  ( $x = 2, 3$ ),  $\text{Sb}_y^-$  ( $y = 1-3, 9$ ), and  $\text{Te}_z^-$  ( $z = 1-5$ ) clusters were also observed.

Only one series of  $\text{Te}_z^+$  ( $z = 1-5$ ) clusters was detected for thin film 'K' since it consisted of 100% Te. The stoichiometry of the clusters was determined via the comparison of the experimental and theoretical isotopic patterns. For example, a comparison of the experimental and theoretical mass spectra recorded via LA for the thin films is shown in Figures 5A and B.

Similarly, the highest number of binary clusters (13 clusters) was detected for thin film 'E,' with a higher content of Te (41.6 at. %) than Sb (6.5 at. %), while the lowest number of binary clusters (4 clusters) was noticed for thin films 'B,' 'C' ( $\text{GaTe}^-$ ,  $\text{GaTe}_2^-$ ,  $\text{SbTe}^-$ , and  $\text{SbTe}_2^-$ ), and 'F' ( $\text{GaTe}^-$ ,  $\text{GaTe}_2^-$ ,  $\text{GaTe}_3^-$ , and  $\text{GaTe}_4^-$ ) with the lowest Te content of 11.5-46.9 at. %. The two ternary  $\text{Ga}_x\text{Sb}_y\text{Te}_z^-$  ( $x = 1, 2, y = 1, z = 2$ ) clusters were recorded only for thin film 'H,' with the lowest Te content (24.7 at. %). In contrast to the positive ion mode, one unary  $\text{Sb}_3^-$  and one binary  $\text{GaSb}_2^-$  cluster were observed for thin film 'A,' which did not contain Te. The cluster with the lowest mass,  $\text{GaTe}^-$ , was identified for all thin films with Te composition  $\geq 11.5$  at. %, i.e., 'B-J,' while the cluster with the highest mass was not the same for all films. The clusters with the highest masses, namely,  $\text{SbTe}_2^-$ ,  $\text{GaSb}_8^-$ ,  $\text{Ga}_2\text{Sb}_{15}^-$ ,  $\text{GaTe}_4^-$ , and  $\text{SbTe}_3^-$ , which were detected for thin films 'B,' 'C,' and 'G' (with Te content of 11.5-22.2 at. %), 'D,' 'E,' and 'F' ( $\text{Sb} \geq 0$  at. %), and 'H-J' ( $\text{Te} \geq 24.7$  at. %), respectively. In contrast to the positive ion mode, the peaks intensities of the clusters with the lowest masses for all thin films were higher than those of the clusters with the highest masses here.

## 4 | DISCUSSION

### 4.1 | Comparison of the stoichiometry of clusters detected in positive and in negative ion modes

The stoichiometries of the clusters generated via LA in positive ion mode are marginally distinct from those generated in negative ion mode. In negative ion mode, slightly higher numbers of clusters and more intensive mass spectra are observed, as compared to the positive ion mode. Similar mass spectra resolution ( $\sim 6000$ ) was found for both positive and negative ion modes.

The overview of the  $\text{Ga}_x\text{Sb}_y\text{Te}_z^{+/-}$  clusters generated in the plasma plume of the eleven thin films A-K (with Te content in the range 0-100 at. %) consisting of various chemical composition is given in Tables S1A and B. Some minor (low-intensity) peaks of oxidized as well as hydrogenated or oxidized/hydrogenated clusters were also detected for the thin films (e.g.,  $\text{SbO}_2^-$ ,  $\text{SbTeO}^-$ ,

$\text{Ga}_2\text{Sb}_7\text{O}^-$ ,  $\text{GaSb}_8\text{O}^-$ ,  $\text{SbTe}_2\text{H}_7^-$ ,  $(\text{Ga}_2\text{H}_6)_2\text{TeH}^-$ ,  $(\text{Ga}_2\text{H}_6)_2\text{Te}^-$ ,  $\text{GaSb}_8\text{O}_2\text{H}_2^-$ , and so on). Digallane ( $\text{Ga}_2\text{H}_6$ ) is well known, and it was also detected as a mixed cluster with other ions in this work (Figure S1). Hydrogen is probably coming from commercial antimony as it is used to synthesize metallic antimony in the redox process. Hydroxy groups are possibly coming from traces of water vapor and oxygen from the environment. Therefore, it can be suggested that the fabricated thin films are containing traces of such impurities (oxides, hydrides, and oxoacids), which were then detected in the MS analyses.

The distribution of binary ( $\text{Ga}_x\text{Sb}_y^{+/-}$ ,  $\text{Ga}_x\text{Te}_z^{+/-}$ , and  $\text{Sb}_y\text{Te}_z^{+/-}$ ) and ternary ( $\text{Ga}_x\text{Sb}_y\text{Te}_z^{+/-}$ ) clusters generated in both positive and negative ion modes from the individual thin film can be seen in Tables S1A and B. The  $\text{Ga}_x\text{Sb}_y^+$  and  $\text{Ga}_x\text{Sb}_y^-$  clusters were observed for the ‘**B**,’ ‘**D**,’ and ‘**E**’ thin films, which have the highest Ga content (49.0-51.9 at. %), and the ‘**A**,’ ‘**D**,’ and ‘**E**’ thin films, which have lower Te content (0-41.6.0 at. %) than Ga content (49.0-51.9 at. %), respectively. Similarly, the  $\text{Ga}_x\text{Te}_z^+$  and  $\text{Ga}_x\text{Te}_z^-$  clusters were detected for thin films ‘**D-F**’ (with the lowest content of Sb: 0-19.6 at. %), ‘**H**’ (the lowest content of Te: 24.7 at. %), and ‘**J**’ (the highest content of Te: 66.7 at. %) and ‘**B-J**’ (all with concentration of Te  $\geq$  11.5 at. %), respectively. All thin films (**B-E**, **G-J**), excluding thin films ‘**A**’ (do not contain Te) and ‘**F**’ (do not contain Sb), with Te content  $\geq$  11.5 at. % generated  $\text{Sb}_y\text{Te}_z^{+/-}$  clusters. Interestingly, only a few thin films, namely, ‘**D**,’ ‘**E**’ (with the highest Ga content: 49.0-51.9 at. %), ‘**H**’ (with the lowest content of Te: 24.7 at. %), ‘**I**,’ and ‘**J**’ (with the lowest concentration of Ga: 27.4, 16.6 at. %) generate ternary  $\text{Ga}_x\text{Sb}_y\text{Te}_z^+$  clusters, while  $\text{Ga}_x\text{Sb}_y\text{Te}_z^-$  clusters are observed only for thin film ‘**H**,’ which has the lowest Te content (24.7 at. %) in the negative ion mode. Note that only one binary cluster was detected for thin film ‘**A**’ (content: Ga 48.0 at. %, and Sb 52.0 at. %). It is possible that there is a strong binding between Ga and Sb that retards the ionization of their thin film under irradiation by the laser pulse. It seems that the highest number (16-19) of clusters is detected for thin films containing high concentration of Te (thin films ‘**E**’ (41.6 at. %) and ‘**J**’ (66.7 at. %)) in both positive and negative ion modes. However, the intensities of the peaks corresponding to clusters vary according to the chemical composition of the thin films.

For the sake of clarity, a summary of the  $\text{Ga}_x\text{Sb}_y\text{Te}_z$  clusters generated via LA from the Ga-Sb-Te thin films ‘**A-K**’ (with Te content in the range of 0-100 at. %) in both the positive and negative ion modes is shown in Table 2. It shows that higher numbers of  $\text{Ga}_x\text{Te}_z$  and  $\text{Ga}_x\text{Sb}_y\text{Te}_z$  clusters are detected in the positive ion mode than in the negative one, while higher numbers of  $\text{Ga}_x\text{Sb}_y$  and

$\text{Sb}_y\text{Te}_z$  clusters are observed in the negative ion mode compared to the positive one. The intensities of mass spectra recorded in negative ion mode are higher than those recorded in the positive one. This trend prevails due to the electronegativity of the elements (Ga, Sb, and Te) present in the thin films.

Moreover, it was shown that the peaks intensities of the detected clusters vary according to the chemical composition of the thin films. To verify this, we selected some of the common clusters identified for thin films 'B-F' (Te content increased from 11.5 to 46.9 at. %) and assigned their chemical composition to line 1, then did the same for thin films 'G-J' (Te content increased from 12.4 to 100 at. %) and assigned their chemical composition to line 2 (Figure 1). Next, we plotted their peaks intensities versus chemical composition (or thin films), as shown in Figures S2A and B. The figure demonstrates that for the peak's intensities of the  $\text{GaTe}_2^-$  (for thin films B-F) and  $\text{SbTe}_2^-$  (for thin films B-E) clusters on line 1 (Figure 1), the chemical composition of the thin films increases as the Te content increases from 11.5 to 46.9 at. % (Figure S2A). Again, the peaks intensities increase for the thin films 'G-J' corresponding to line 2 (Figure 1) as the concentration of Te increases from 12.4 to 66.7 at. % (Figure S2B). Similarly, the peak intensity of the  $\text{GaTe}^-$  cluster increases for thin films 'C' and 'D' as the Te content increases from 11.5 to 31.4 at. % (Figure S2A). Its peak intensity also increases for the thin films 'G,' 'H,' and 'J' as the Te content increases from 12.4 to 66.7 at. % (Figure S2B). Naturally, the peaks intensities of the clusters  $\text{GaTe}^-$ ,  $\text{GaTe}_2^-$ , and  $\text{SbTe}_2^-$  increase when the Te concentration in thin films increases.

The determination of the structure of the  $\text{Ga}_x\text{Sb}_y\text{Te}_z$  clusters is not possible from mass spectra itself. However, when looking for the relationship between the generated clusters and the structure of the thin films fabricated in this work, the results show that at least some of the structural units identified as clusters might correspond to the structural units of thin films reported for the crystalline  $\text{Ga}_4\text{Sb}_6\text{Te}_3$  phase change compound and amorphous and crystallized Ge-Sb-Te thin films in the literature.<sup>32,33</sup> For example, the  $\text{SbTe}_3$  pyramidal structural unit has been identified for both the  $\text{Ga}_4\text{Sb}_6\text{Te}_3$  phase change compound and Ge-Sb-Te thin films. This pyramidal structural unit corresponds to the  $\text{SbTe}_3^-$  cluster detected for the thin films fabricated in this work, thus confirming the presence of the  $\text{SbTe}_3$  pyramidal unit in the original structures of fabricated thin films. Moreover, the structure(s) of the crystalline GaTe and/or  $\text{Ga}_4\text{Sb}_6\text{Te}_3$  phase change materials have already been reported (Figure S3).<sup>23,33</sup> Here, the detected clusters appear to be the fractions

of the structures of the parent thin films (Figure S3). Interferences of some reactions in the plasma plume are probably low and can be neglected.<sup>34</sup>

## 4.2 | Suppression of clusters fragmentation

Naturally, the clusters observed are formed by destruction of the thin film structure during laser ablation. As it was mentioned in the “Introduction” we have observed that covering the samples with a thin layer of paraffin’s often increases considerably mass spectra intensity and even new clusters are sometimes observed.<sup>25,28,29</sup> This effect has not been sufficiently explained up to now – this is why we examined here in detail this “paraffin’s effect” and also the use of some other agents like glycerol and trehalose (non-reducing sugar) has been examined. The studied compounds have a common feature that they are difficult to ionize.<sup>35</sup>

The mass spectra of selected thin films, namely, ‘**A**,’ ( $\text{Ga}_{48.0}\text{Sb}_{52.0}$ ), ‘**F**,’ ( $\text{Ga}_{53.1}\text{Sb}_{46.9}$ ), and ‘**I**,’ ( $\text{Ga}_{27.4}\text{Sb}_{29.0}\text{Te}_{43.6}$ ) - coated either with paraffin’s, glycerol, or trehalose layer were recorded in both positive and negative ion modes. The results show that the stoichiometry of clusters generated from coated thin films was apparently different as compared to those generated from uncoated films. For example,  $\text{Sb}^-$  and  $\text{Sb}_2^-$  clusters were detected from thin film ‘**A**,’ ( $\text{Ga}_{48.0}\text{Sb}_{52.0}$ ) coated with paraffin’s layer and  $\text{Sb}^-$  cluster was from thin film ‘**A**,’ coated with trehalose layer. Similarly,  $\text{Ga}_3\text{Te}^-$  cluster was identified from thin film ‘**F**,’ ( $\text{Ga}_{53.1}\text{Te}_{46.9}$ ) coated with paraffin’s layer. Cluster  $\text{Ga}_2\text{Te}^+$  was obtained from thin film ‘**I**,’ ( $\text{Ga}_{27.4}\text{Sb}_{29.0}\text{Te}_{43.6}$ ) coated with trehalose layer and  $\text{Ga}_3\text{SbTe}_3\text{H}_7^-$  cluster was from thin film ‘**I**,’ coated with paraffin’s layer. The intensities of mass spectra recorded from coated thin films were almost always higher than those generated from uncoated films. The intensities of mass spectra concerning clusters generated from coated thin films increased 3-30 $\times$  as compared to those from uncoated thin films. An example of the comparison between mass spectra intensities recorded from uncoated and coated thin films **I** and **F** is shown in Figures 6A and B.

The effect of examined compounds (paraffin’s, glycerol, and trehalose) on thin film mass spectra is certainly complex. The deposited layer on thin films is first evaporated with laser and gaseous molecules of the additives might work in plasma plume as absorber material decreasing considerably energy of excited cluster ions. As a consequence, fragmentation of the clusters is diminished. In addition, coating can be during the laser ablation partially decomposed into smaller molecules (e.g.,  $\text{CO}_2$ ,  $\text{H}_2\text{O}$ , and others from trehalose sugar) and these molecules contribute to the

formation of a dense environment in plasma plume which could “collisionally” calm the clusters and slow down the rate of their decay.<sup>30</sup> Finally, the increased population of long-lived ions is available in plasma plume and/or during the time of flight in a tube of mass spectrometer. Consequently, the increased intensity of mass spectra recorded from coated thin film is observed and some peaks not observed before (because of total fragmentation) are visualized with elevated intensity.

## 5 | CONCLUSION

Ga-Sb-Te chalcogenide thin films prepared using the RF magnetron co-sputtering technique with GaSb, GaTe, and Te targets were found to be amorphous. This kind of thin films has most likely been studied here for the first-time using mass spectrometry. LA of these thin films generates unary ( $\text{Ga}_x^{+/-}$ ,  $\text{Sb}_y^{+/-}$ , and  $\text{Te}_z^{+/-}$ ), binary ( $\text{Ga}_x\text{Sb}_y^{+/-}$ ,  $\text{Ga}_x\text{Te}_z^{+/-}$ , and  $\text{Sb}_y\text{Te}_z^{+/-}$ ), and ternary ( $\text{Ga}_x\text{Sb}_y\text{Te}_z^{+/-}$ ) clusters. The intensities of the mass spectra acquired in the negative ion mode are higher than those obtained in the positive one. Peak's intensities are varied according to the chemical composition of the thin films. For example, the intensities of the peaks corresponding to the  $\text{GaTe}_2^-$  and  $\text{SbTe}_2^-$  (for thin films from GaSb-GaTe tie line) species increase as the Te content increases from 11.5 to 46.9 at. %. Again, peaks intensities are increased for thin films from GaSb-Te tie line when the Te content increases from 12.4 to 66.7 at. %. The intensities of mass spectra recorded from thin films coated with paraffin's, glycerol, or trehalose were found in several cases much higher (30 x) than those of mass spectra recorded from uncoated films. It can be explained by the fact that the degraded smaller molecules of glycerol, paraffin's or trehalose sugar are absorbing part of the energy of excited ions in the plasma plume and thus the fragmentation of the cluster ions is suppressed, and an increased population of longer-lived ions is obtained and in this way, increased signal sensitivities are reached. The finding of such molecules suppressing the fragmentation, we consider as quite an important achievement for mass spectrometry of not only chalcogenides.

The number of clusters identified for the positive (28 clusters) and negative (32 clusters) ion modes is similar. In total, 41 clusters of different stoichiometry's were observed. The highest number (18) of binary and ternary clusters was found for thin film with composition  $\text{Ga}_{51.9}\text{Sb}_{6.5}\text{Te}_{41.6}$ , while the lowest number of clusters was observed for thin film with low content of Te, i.e., for  $\text{Ga}_{43.1}\text{Sb}_{44.5}\text{Te}_{12.4}$  thin film.

In conclusion, the deposition technique used in this study allows thin films with a wide range of chemical composition to be fabricated. LA QIT TOF MS proved to be an important and useful analytical method for studying chalcogenide thin films in terms of stoichiometry estimations for clusters present in plasma plume when thin films are irradiated with laser pulses. The increased intensities of mass spectra can be achieved using a layer of energy absorber materials on the surface of thin films. The identified clusters represent anyway fragmented entities of the local structure of thin films. Determined stoichiometry of clusters may be useful as the structural characterizations of thin films and might help in the development of new phase change or other advanced materials.

#### **ACKNOWLEDGEMENTS**

This work was supported by the Czech Science Foundation (Project No. 19-24516S) and by Platform Spectroscopy Infrared and Raman (SIR – ScanMAT, Université De Rennes 1). G. M. is grateful for the financial support received from Project No. MUNI/A/1421/2019 for the Analytical and Physical and Chemical Methods for Geological, Biological and Synthetic Materials.

## REFERENCES

1. Raoux S, Welnic W, Lelmini D. Phase change materials and their application to nonvolatile memories. *Chem Rev.* 2010;110(1):240–67.
2. Lencer D, Salinga M, Wuttig M. Design rules for phase-change materials in data storage applications. *Adv Mater.* 2011;23(18):2030–58.
3. Deringer VL, Dronskowski R, Wuttig M. Microscopic complexity in phase-change materials and its role for applications. *Adv Funct Mater.* 2015;25(40):6343–59.
4. Zhang W, Mazzarello R, Wuttig M, Ma E. Designing crystallization in phase-change materials for universal memory and neuro-inspired computing. *Nat Rev Mater.* 2019;4(3):150–68.
5. Nazir H, Batool M, Bolivar Osorio FJ, Isaza-Ruiz M, Xu X, Vignarooban K, et al. Recent developments in phase change materials for energy storage applications: A review. *Int J Heat Mass Transf.* 2019;129:491–523.
6. Yang Z, Ramanathan S. Breakthroughs in photonics 2014: Phase change materials for photonics. *IEEE Photonics J.* 2015;7(3):0700305.
7. Lee SY, Kim YH, Cho SM, Kim GH, Kim TY, Ryu H, et al. Holographic image generation with a thin-film resonance caused by chalcogenide phase-change material. *Sci Rep.* 2017;7:41152.
8. Yamada N. Origin, secret, and application of the ideal phase-change material GeSbTe. *Phys Status Solidi Basic Res.* 2012;249(10):1837–42.
9. Bouška M, Pechev S, Simon Q, Boidin R, Nazabal V, Gutwirth J, et al. Pulsed laser deposited GeTe-rich GeTe-Sb<sub>2</sub>Te<sub>3</sub> thin films. *Sci Rep.* 2016;6:26552.
10. Buller S, Koch C, Bensch W, Zalden P, Sittner R, Kremers S, et al. Influence of partial substitution of Te by Se and Ge by Sn on the properties of the blu-ray phase-change material Ge<sub>8</sub>Sb<sub>2</sub>Te<sub>11</sub>. *Chem Mater.* 2012;24(18):3582–90.
11. Kao KF, Lee CM, Chen MJ, Tsai MJ, Chin TS. Ga<sub>2</sub>Te<sub>3</sub>Sb<sub>5</sub>-A candidate for fast and ultralong retention phase-change memory. *Adv Mater.* 2009;21(17):1695–9.
12. Cheng HY, Kao KF, Lee CM, Chin TS. Characteristics of Ga-Sb-Te films for phase-change memory. *IEEE Trans Magn.* 2007;43(2):927–9.
13. Cheng HY, Raoux S, Jordan-Sweet JL. The crystallization behavior of stoichiometric and

- off-stoichiometric Ga-Sb-Te materials for phase-change memory. *Appl Phys Lett*. 2011;98(12):121911.
14. Lu Y, Song S, Song Z, Ren W, Cheng Y, Liu B. Crystallization process of amorphous GaSb<sub>5</sub>Te<sub>4</sub> film for high-speed phase change memory. *Appl Phys Express*. 2011;4(9):094102.
  15. Lee CM, Lin YI, Chin TS. Crystallization kinetics of amorphous Ga-Sb-Te films: Part II. Isothermal studies by a time-resolved optical transmission method. *J Mater Res*. 2004;19(10):2938–46.
  16. Bouška M, Nazabal V, Gutwirth J, Halenkovič T, Přikryl J, Normani S, et al. GaTe–Sb<sub>2</sub>Te<sub>3</sub> thin-films phase change characteristics. *Opt Lett*. 2020;45(5):1067-70.
  17. Park H, Nam S, Shin C, Kim J. Infrared thermal detector and method of manufacturing the same. 2015;U.S. Patent No. 9,091,591.
  18. Lee CM, Lin YI, Chin TS. Crystallization kinetics of amorphous Ga-Sb-Te chalcogenide films: Part I. Nonisothermal studies by differential scanning calorimetry. *J Mater Res*. 2004;19(10):2929–37.
  19. Němec P, Takats V, Csik A, Kokenyesi S. GeSe/GeS nanomultilayers prepared by pulsed laser deposition. *J Non Cryst Solids*. 2008;354(52–54):5421–4.
  20. Mane RS, Lokhande CD. Chemical deposition method for metal chalcogenide thin films. *Mater Chem Phys*. 2000;65(1):1–31.
  21. García-García E, Mendoza-Galván A, Vorobiev Y, Morales-Sánchez E, González-Hernández J, Martínez G, et al. Optical properties of Ge:Sb:Te ternary alloys. *J Vac Sci Technol A Vacuum, Surfaces, Film*. 1999;17(4):1805–10.
  22. Lee CM, Yen WS, Chen JP, Chin TS. Performances of phase-change recording disks based on GaSbTe media. *IEEE Trans Magn*. 2005;41(2):1022–4.
  23. Bouzid A, Gabardi S, Massobrio C, Boero M, Bernasconi M. First-principles study of amorphous Ga<sub>4</sub>Sb<sub>6</sub>Te<sub>3</sub> phase-change alloys. *Phys Rev B - Condens Matter Mater Phys*. 2015;91(18):184201.
  24. Mawale R, Mandal G, Bouška M, Gutwirth J, Bora PL, Nazabal V, et al. Amorphous Ge-Bi-Se thin films: A mass spectrometric study. *Sci Rep*. 2019;9(1):19168.
  25. Mawale R, Halenkovič T, Bouška M, Gutwirth J, Nazabal V, Bora PL, et al. Mass spectrometric investigation of amorphous Ga-Sb-Se thin films. *Sci Rep*. 2019;9(1):10213.
  26. Pangavhane SD, Němec P, Nazabal V, Moreac A, Jövári P, Havel J. Laser desorption

- ionization time-of-flight mass spectrometry of erbium-doped Ga-Ge-Sb-S glasses. *Rapid Commun Mass Spectrom.* 2014;28(11):1221–32.
27. Houška J, Peña-Méndez EM, Kolář J, Přikryl J, Pavlišta M, Frumar M, et al. Laser desorption time-of-flight mass spectrometry of atomic switch memory  $\text{Ge}_2\text{Sb}_2\text{Te}_5$  bulk materials and its thin films. *Rapid Commun Mass Spectrom.* 2014;28(7):699–704.
28. Mandal G, Mawale RM, Gutwirth J, Nemeč P, Havel J. Laser ablation generation of bismuth selenide clusters from mixtures of elements, crystalline  $\text{Bi}_2\text{Se}_3$ , or thin films: Laser desorption ionization (LDI) and surface assisted LDI time-of-flight mass spectrometry using graphene and nanodiamonds. *J Am Soc Mass Spectrom.* 2020;31(1):66–72.
29. Mawale RM, Ausekar MV, Prokeš L, Nazabal V, Baudet E, Halenkovič T, et al. Laser desorption ionization of  $\text{As}_2\text{Ch}_3$  (Ch = S, Se, and Te) chalcogenides using quadrupole ion trap time-of-flight mass spectrometry: A comparative study. *J Am Soc Mass Spectrom.* 2017;28(12):2569–79.
30. Shahgholi M, Garcia BA, Chiu NHL, Heaney PJ, Tang K. Sugar additives for MALDI matrices improve signal allowing the smallest nucleotide change (A:T) in a DNA sequence to be resolved. *Nucleic Acids Res.* 2001;29(19):e91.
31. Halenkovič T, Gutwirth J, Nemeč P, Baudet E, Specht M, Gueguen Y, et al. Amorphous Ge-Sb-Se thin films fabricated by co-sputtering: Properties and photosensitivity. *J Am Ceram Soc.* 2018;101(7):2877–87.
32. Nemeč P, Nazabal V, Moreac A, Gutwirth J, Beneš L, Frumar M. Amorphous and crystallized Ge-Sb-Te thin films deposited by pulsed laser: Local structure using Raman scattering spectroscopy. *Mater Chem Phys.* 2012;136(2–3):935–41.
33. Baratella D, Dragoni D, Ceresoli D, Bernasconi M. First-principles study on the crystalline  $\text{Ga}_4\text{Sb}_6\text{Te}_3$  phase change compound. *Phys Status Solidi - Rapid Res Lett.* 2021;15(3):2000382.
34. Mawale R, Halenkovič T, Bouška M, Gutwirth J, Nazabal V, Takáts V, et al. Laser desorption ionization time-of-flight mass spectrometry of  $\text{Ge}_x\text{Se}_{1-x}$  chalcogenide glasses, their thin films, and Ge:Se mixtures. *J Non Cryst Solids.* 2019;509:65–73.
35. Yang M, Hashimoto K, Fujino T. Silver nanoparticles loaded on ammonium exchanged zeolite as matrix for MALDI-TOF-MS analysis of short-chain *n*-alkanes. *Chem Phys Lett.* 2018;706:525–32.

### Captions to the figures

**FIGURE 1** Chemical composition (at. %) of fabricated Ga-Sb-Te thin films (A-K). Lines 1 and 2 are guiding the eye for co-sputtering using GaSb-GaTe and GaSb-Te targets, respectively

**FIGURE 2** Effect of the laser energy on the generation of clusters via the LA of thin film J. Conditions: negative ion mode,  $m/z$  range 100-400, intensities in  $m/z$  ranges 120-180 and 340-400 were magnified 10 times, 2000 profiles, and 100% intensity corresponding to 1964 mV

**FIGURE 3** Comparison of the mass spectra generated via LA from thin films (A-J). Conditions: negative ion mode, laser energy 160 a.u.,  $m/z$  range 100-400, 2000 profiles

**FIGURE 4** Comparison of the mass spectra intensities recorded via LA for thin film E in positive and negative ion modes. Conditions: laser energy 160 a.u.;  $m/z$  range 100-500; intensity in  $m/z$  range 100-190 was magnified two times, while it was magnified 10 times in the  $m/z$  350-500 range; 2000 profiles

**FIGURE 5** (A) Comparison of the experimental and theoretical mass spectra recorded via LA for thin film J. Conditions: negative ion mode, laser energy 150 a.u.,  $m/z$  range 150-400, intensity in  $m/z$  range 360-400 was magnified 10 times, 2000 profiles, and 100% intensity corresponds to 880 mV and (B) comparison of the experimental and theoretical mass spectra recorded via LA for thin film E. Conditions: negative ion mode, laser energy 150 a.u.,  $m/z$  range 1000-1090, intensity in the  $m/z$  range 1000-1055 was magnified two times, 2000 profiles, and 100% intensity corresponds to 11 mV

**FIGURE 6** (A) Comparison of intensities of mass spectra recorded via LA from uncoated and coated thin films I. Conditions: negative ion mode, laser energy 160 a.u., and 2000 profiles and (B) comparison of mass spectra intensities recorded via LA from uncoated and coated thin films F. Conditions: negative ion mode, laser energy 150 a.u., and 2000 profiles

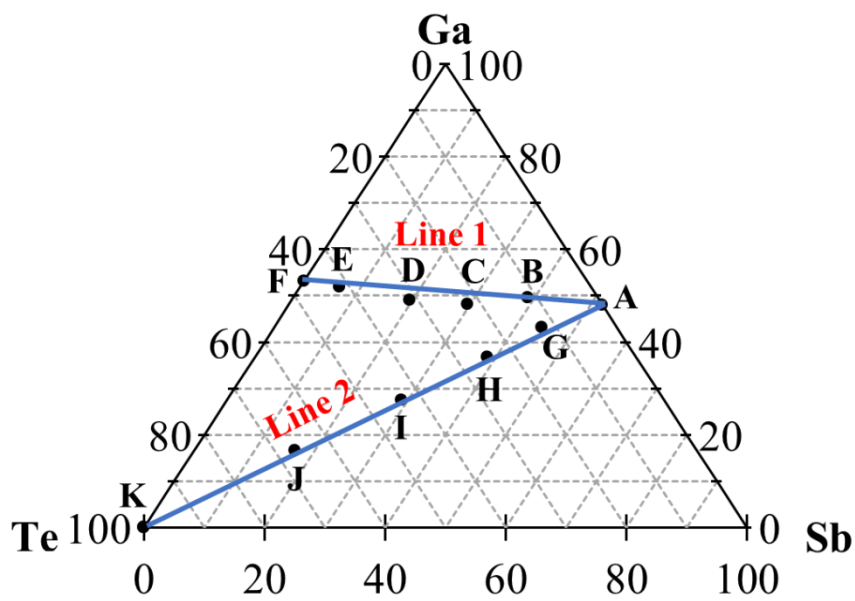
**TABLE 1** Thin film identification, RF sputtering power applied on individual cathodes, and chemical composition of the fabricated Ga-Sb-Te thin films determined via EDS analysis ( $\pm 1$  at. %)

Thin film	RF power (W)			Chemical composition (at. %)		
	GaSb	GaTe	Te	Ga	Sb	Te
<b>A</b>	15	-	-	48.0	52.0	0
<b>B</b>	21	10	-	49.5	39.0	11.5
<b>C</b>	16	14	-	48.2	29.6	22.2
<b>D</b>	12	18	-	49.0	19.6	31.4
<b>E</b>	7	23	-	51.9	6.5	41.6
<b>F</b>	-	15	-	53.1	0	46.9
<b>G</b>	35	-	4	43.1	44.5	12.4
<b>H</b>	30	-	6	36.6	38.7	24.7
<b>I</b>	25	-	9	27.4	29.0	43.6
<b>J</b>	20	-	15	16.6	16.7	66.7
<b>K</b>	-	-	10	0	0	100.0

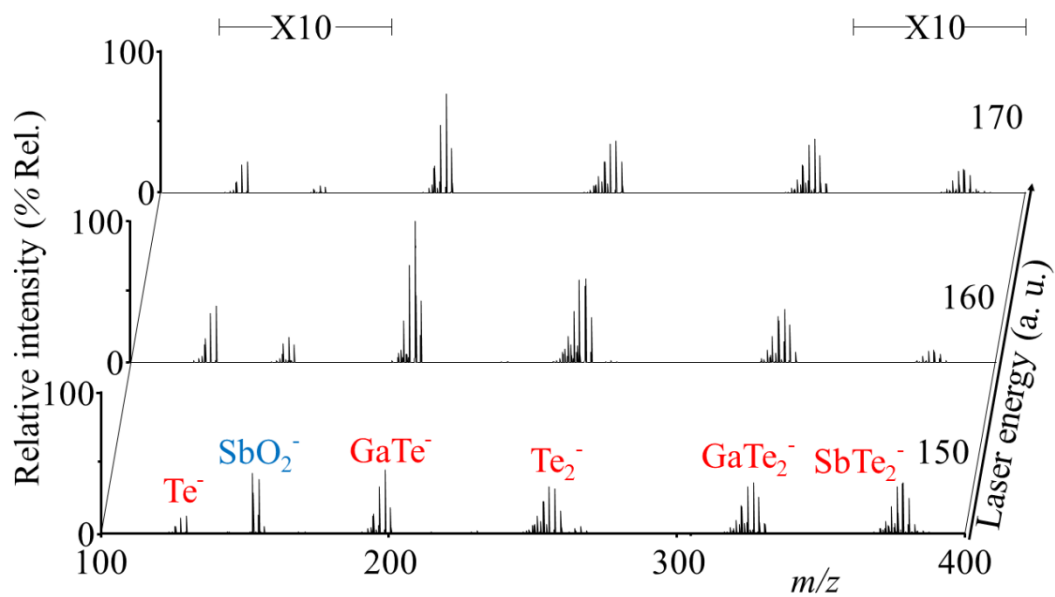
**TABLE 2** Summary of  $\text{Ga}_x\text{Sb}_y\text{Te}_z$  clusters generated via LA from all Ga-Sb-Te thin films (A-K) in both positive and negative ion modes

$\text{Ga}_x$	$\text{Sb}_y$	$\text{Te}_z$	$\text{Ga}_x\text{Sb}_y$	$\text{Ga}_x\text{Te}_z$	$\text{Sb}_y\text{Te}_z$	$\text{Ga}_x\text{Sb}_y\text{Te}_z$
$\text{Ga}_2^{+/-}$	$\text{Sb}^{+/-}$	$\text{Te}^{+/-}$	$\text{GaSb}^+$	$\text{GaTe}^{+/-}$	<b><math>\text{SbTe}^{+/-}</math></b>	<b><math>\text{GaSbTe}^+</math></b>
$\text{Ga}_3^-$	$\text{Sb}_2^-$	$\text{Te}_2^{+/-}$	$\text{GaSb}_2^-$	<b><math>\text{GaTe}_2^{+/-}</math></b>	$\text{Sb}_2\text{Te}^{+/-}$	$\text{GaSbTe}_2^{+/-}$
	$\text{Sb}_3^{+/-}$	$\text{Te}_3^{+/-}$	<b><math>\text{GaSb}_8^{+/-}</math></b>	$\text{GaTe}_3^{+/-}$	$\text{Sb}_3\text{Te}^+$	$\text{GaSbTe}_3^-$
	$\text{Sb}_4^+$	$\text{Te}_4^{+/-}$	$\text{Ga}_2\text{Sb}^+$	$\text{GaTe}_4^-$	$\text{SbTe}_2^{+/-}$	$\text{GaSb}_2\text{Te}^+$
	$\text{Sb}_9^{+/-}$	$\text{Te}_5^{+/-}$	$\text{Ga}_2\text{Sb}_{15}^-$	$\text{Ga}_2\text{Te}^{+/-}$	$\text{SbTe}_3^-$	$\text{GaSb}_2\text{Te}_2^+$
			$\text{Ga}_3\text{Sb}_{14}^-$	$\text{Ga}_2\text{Te}_2^{+/-}$	$\text{Sb}_2\text{Te}_2^-$	$\text{Ga}_2\text{SbTe}_2^-$
			$\text{Ga}_4\text{Sb}_{13}^-$	$\text{Ga}_3\text{Te}^+$		
			$\text{Ga}_6\text{Sb}_5^-$	$\text{Ga}_3\text{Te}_2^+$		
			$\text{Ga}_7\text{Sb}_4^-$			

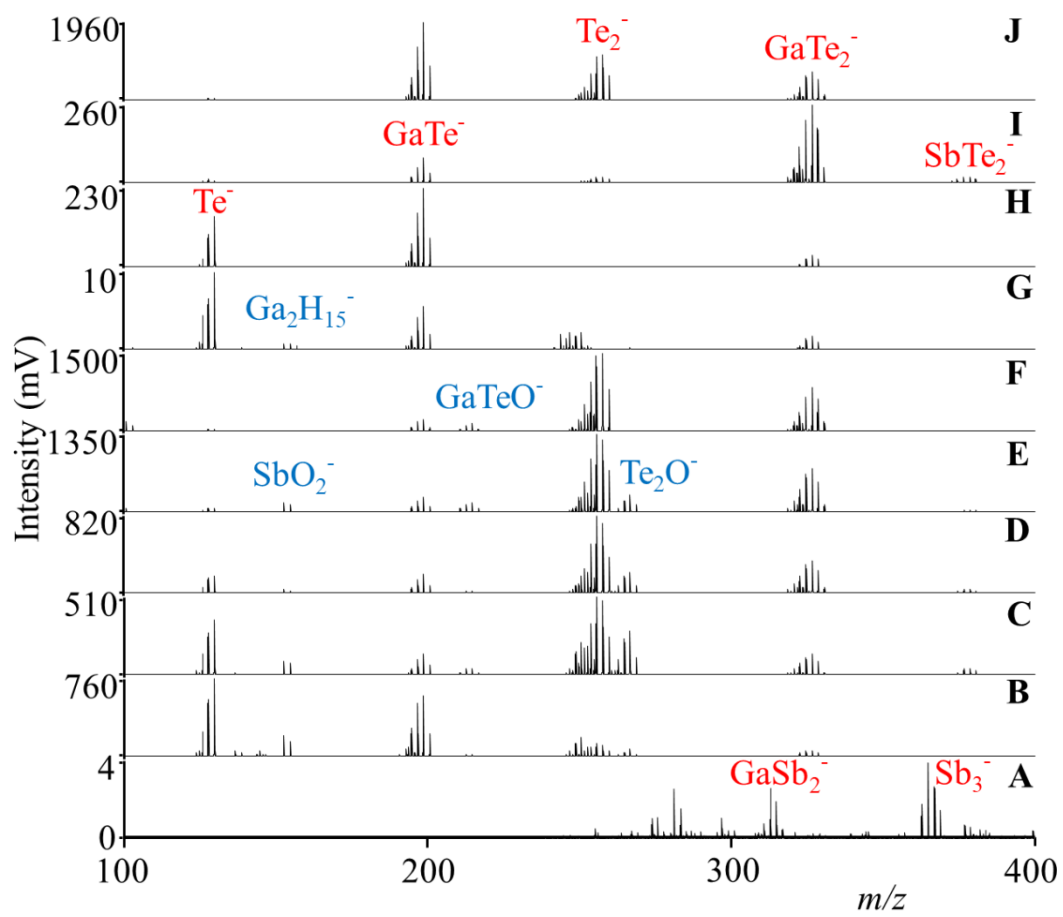
**Remarks:** The symbols + and - mean that clusters were observed in the positive and negative ion modes, respectively, whereas +/- means that clusters were detected in both the positive and negative ion modes. The clusters highlighted in 'BOLD' are the most intensive peaks of binary and ternary clusters. Some minor (low-intensity) peaks of "oxidized and hydrogenated or oxidized/hydrogenated" clusters observed are not mentioned here.



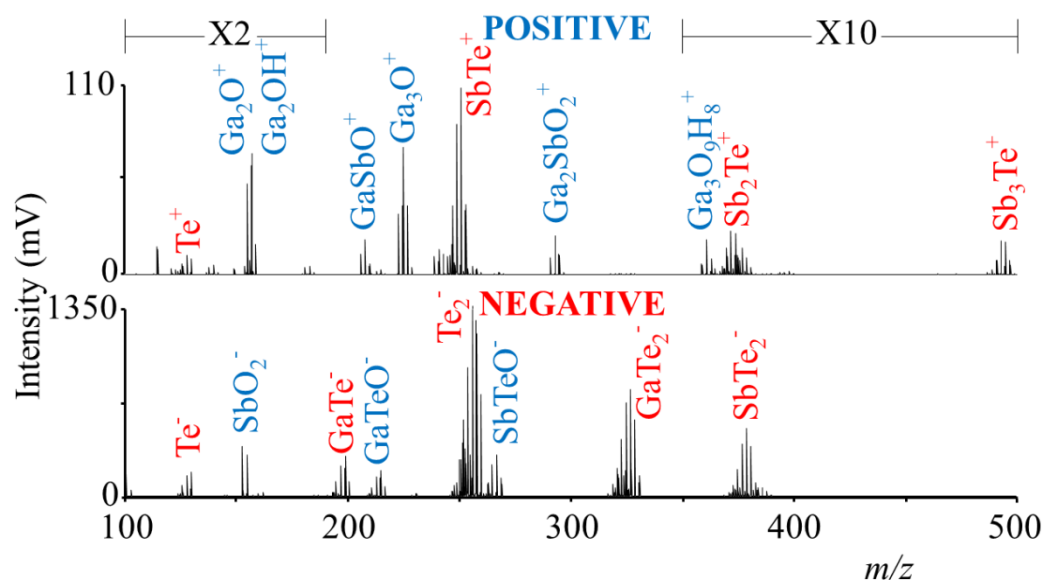
jace\_18021\_f1.tif



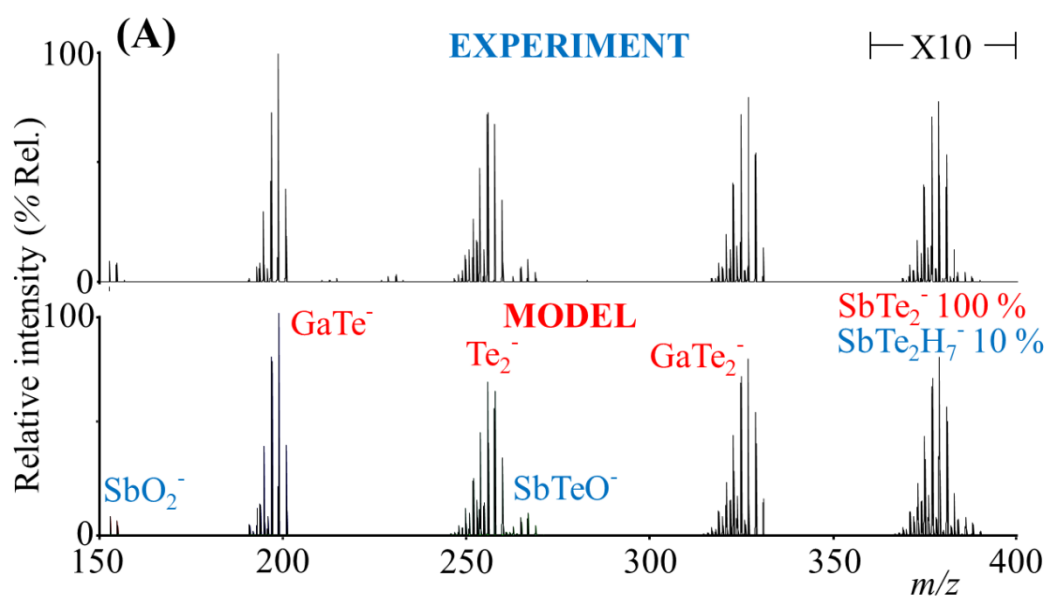
jace\_18021\_f2.tif



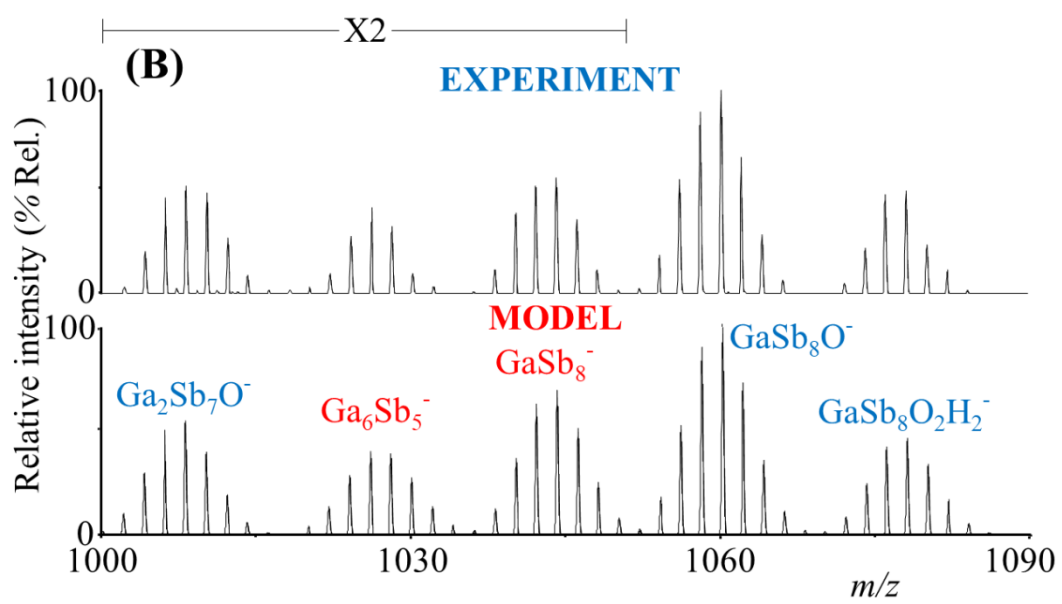
jace\_18021\_f3.tif



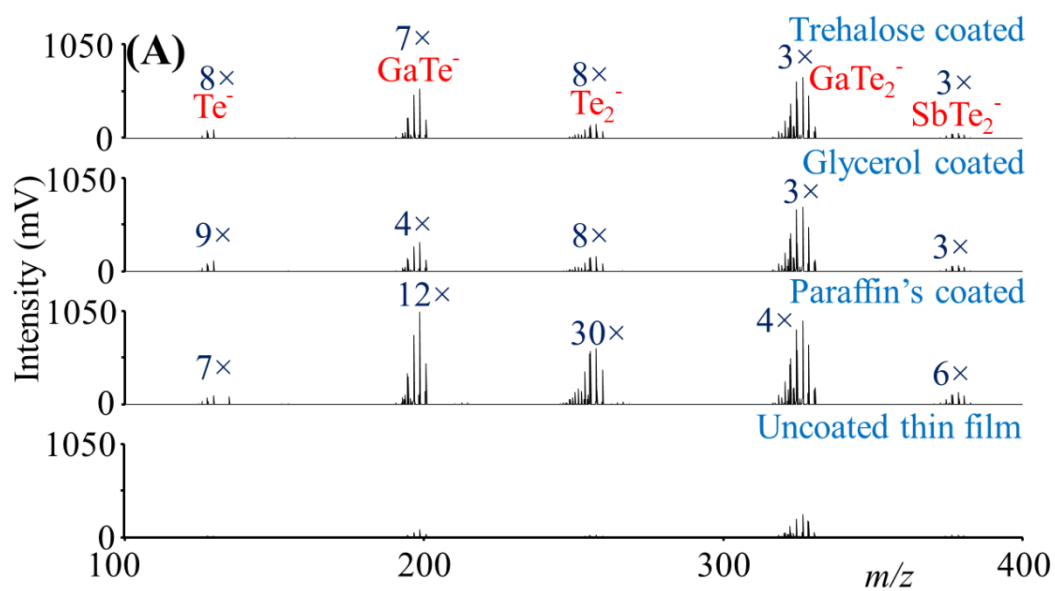
jace\_18021\_f4.tif



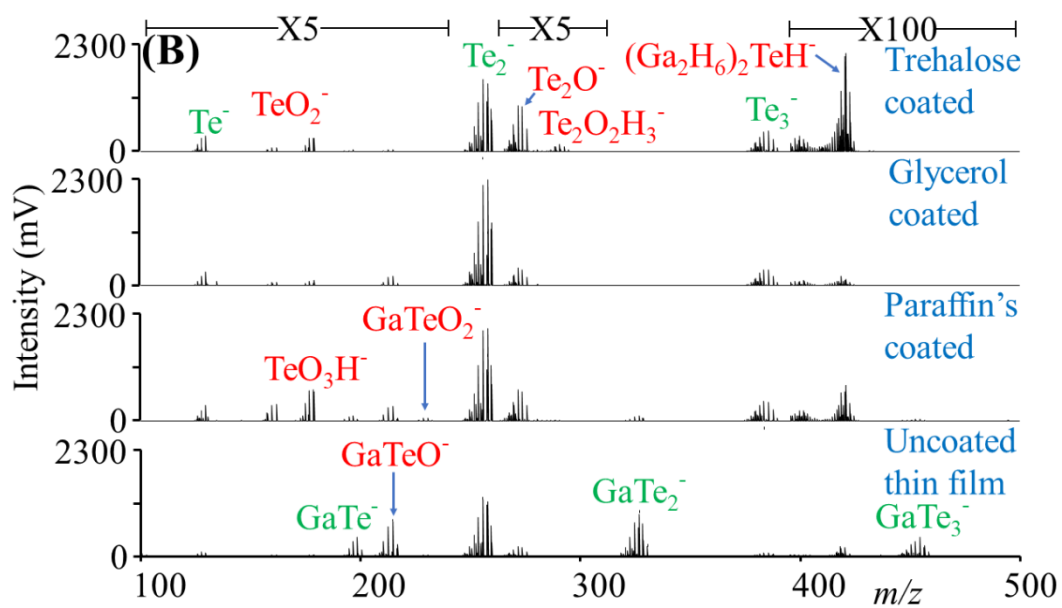
jace\_18021\_f5a.tif



jace\_18021\_f5b.tif



jace\_18021\_f6a.tif



jace\_18021\_f6b.tif